JANUARY 21 2026

Influence of differential rotor speeds on the performance and acoustic emission of coaxial propellers[a)]

Sen Wang ; Lourenço Tércio Lima Pereira ; Riccardo Zamponi ; Daniele Ragni

J. Acoust. Soc. Am. 159, 539–552 (2026)
https://doi.org/10.1121/10.0042251

JASA ARTICLE

Influence of differential rotor speeds on the performance and acoustic emission of coaxial propellers[a)]

Sen Wang,[1,b)] Lourenço Tércio Lima Pereira,[1] Riccardo Zamponi,[1,2] and Daniele Ragni[1]
[1]Department of Flow Physics and Technology, Delft University of Technology, Delft, 2629 HS, The Netherlands
[2]von Karman Institute for Fluid Dynamics, Waterloosesteenweg 72, B-1640 Sint-Genesius-Rode, Belgium

ABSTRACT:
This study investigated the noise emission and thrust performance of a heavy-lift unmanned air vehicle (UAV) with a coaxial propulsion system that operates under differential rotor speeds. The UAV adopted an octo-quad architecture, where each rotor pair consists of two propellers with different blades, allowing independent operation of fore and aft rotors in corotating (CR) and contra-rotating (CTR) configurations. Acoustic emissions and thrust were measured under steady conditions. The study compared the performances of CR and CTR configurations and examined the influence of differential rotor speed on the noise emission of the vehicle under different loads for both configurations. The results indicate that the CTR configuration achieves a maximum load factor 0.28 higher than that of the CR configuration and features lower noise at the same thrust when employing differential rotor speed. For both configurations, the drone's noise was influenced by the aerodynamic characteristics of propellers. Specifically, increasing the fore rotor speed relative to the aft rotor amplifies the noise, whereas increasing the aft rotor speed reduces noise without compromising thrust. Corresponding noise spectra were analyzed across different load factors. The results provide insights that can inform about the optimization of noise emission and performance of UAVs with coaxial propulsion systems.
 https://doi.org/10.1121/10.0042251
(Received 29 April 2025; revised 22 November 2025; accepted 2 January 2026; published online 21 January 2026)
[Editor: James F. Lynch] Pages: 539–552

I. INTRODUCTION

Unmanned air vehicles (UAVs), or drones, are aerial platforms that operate remotely to perform dangerous or impractical missions for manned aircraft.[1,2] These versatile vehicles have experienced rapid market growth in recent years, with applications from surveillance to planetary exploration and search-and-rescue operations.[2] The great demand for UAVs is particularly evident in civilian applications, such as aerial photogrammetry and recreational activities. As of December 2022, more than 1.47×10^6 new recreational operators had registered with the United States (U.S.) Federal Aviation Administration (FAA) since the online registration system was implemented on December 21, 2015.[3]

The growing demand for civilian drones fuels recent research in UAV design, leading to increased exploration of vehicle layouts and propulsion systems. As mandated by the FAA and the European Union Aviation Safety Agency (EASA), civilian drones under the open category must have a maximum takeoff weight under 25 kg. A brief survey of drones within this range reveals that the most widely adopted architecture is a multicopter with a different number of propulsion units.[2,4–6] These multicopters offer superior maneuverability and hovering capability compared to other designs such as fixed-wing drones. The accessibility, versatility, and affordability of multicopters also contribute to their popularity, especially when combined with recent advancements in electric propulsion and innovative operational concepts, i.e., urban air mobility.[7,8]

Despite these advantages, the multicopter design has several drawbacks such as limited flight endurance and payload.[9] In comparison with a single rotor, a coaxial rotor arrangement of equivalent solidity appears to mitigate these drawbacks by improving torque balance, providing redundancy, and enhancing propulsive efficiency without expanding the footprint of the platform.[6,10–12] This arrangement involves stacking more than one propeller along the same rotational axis and has been successfully implemented in fixed-wing aircraft, e.g., Tupolev Tu-95, and helicopters, e.g., Kamov Ka-50.[12] Note that these propellers are often operating on cross shafts at the same speed, and require a complex gear system to achieve the contra-rotating (CTR) motion.

To better understand the origin of the performance gain in coaxial propellers, it is important to examine the underlying aerodynamic mechanisms. A review of previous studies suggests that this gain is closely related to wake dynamics.[13] Hovering investigations have shown that the fore-propeller wake contracts as it convects downstream, allowing the outboard sections of the aft propeller blades to draw in clean air

[a)]This paper is part of the special issue on Advanced Air Mobility Noise: Predictions, Measurements, and Perception.
[b)]Email: S.Wang-2@tudelft.nl

with a slight upwash.[13,14] Compared with two equivalent isolated propellers, this configuration can increase the effective disk area and reduce the induced power.[13] More importantly, the swirling slipstream of the fore propeller contributes to the increase in tangential velocity over the aft-blade sections. This interaction enables the recovery of the swirling kinetic energy as thrust and is commonly known as swirl recovery.[10] An early National Aeronautics and Space Administration (Washington, DC) analytical study suggested that CTR propellers could save approximately 8% energy compared to a single propeller configuration, which generally agrees with the 11% efficiency gain based on several experimental tests simulating a Mach 0.8 cruise at 35 000 feet with various tip speeds.[10]

In spite of their promising performance, it is crucial to recognize that CTR propellers are known to increase noise that is more than proportional to the sum of the noise of the single rotors.[6,15–17] The aerospace community continually seeks to mitigate such noise penalty without compromising performance. Addressing this challenge requires a thorough understanding of the sound-generation mechanisms of coaxial propellers to enable effective noise control. In typical low-speed UAV operations, propellers produce noise that consists of tonal and broadband components. For an isolated propeller, tonal noise arises from the effects of steady and unsteady blade loading as well as air volume displacement caused by rotation, occurring at the harmonics of the blade-passing frequency (BPF).[18] During hovering, maneuvering, or descending flight, unsteady loading can be attributed to the interaction between the blades and tip vortices shed by preceding blades, i.e., blade-vortex interaction (BVI).[19–22] Regarding the broadband component, trailing-edge noise is identified as the primary source for a single propeller[23,24] and it is associated with turbulence-induced pressure fluctuations that are scattered at the blade's trailing edge.[25]

Building on this, introducing a second row of CTR blades creates additional noise sources as aerodynamic interactions between the propellers can significantly increase the overall noise.[26] Specifically, the aft-propeller blades experience unsteady loading as they periodically cut through the tip vortices produced by the fore propeller.[27] In addition, potential-field interaction is another source of increased tonal noise, wherein each row of blades produces upwash and downwash that impose unsteady loading on the adjacent row of blades.[27] Analytical[28,29] and experimental[6] investigations on CTR noise confirmed that propeller interactions can generate additional tones beyond those BPF tones produced by a single propeller. For the same thrust, the sound pressure level (SPL) amplitudes of the interaction tones could be 30 dB higher than those of the BPF tones.[6] In addition to the tonal component, the additional turbulence produced by the fore propeller appears to contribute to broadband noise.[30] This was confirmed by McKay *et al.*,[6] who found that trailing-edge noise is the main source of broadband noise for CTR propellers by comparing the polar directivities between CTR and single propellers. Their results indicate that for the same thrust, CTR propellers produce broadband SPL levels approximately 3.5–5 dB higher than those for single propellers across all directivity angles.[6]

Although much of the research attention has focused on CTR propellers, an alternative coaxial configuration has also been explored with the aim of reducing propeller noise. The effort can be traced back half a century to when Deutsches Zentrum für Luft- und Raumfahrt (Cologne, Germany; DLR) and NASA initiated investigations into unconventional propeller systems, such as those without coplanar blades, equal azimuth spacing, or equal collective pitch, allowing great flexibility in design to improve performance and acoustic characteristics.[31–33] These studies examined corotating (CR) propellers, in which two or three rotors are mounted on the same rotating axis with the fore and aft-propeller blades indexed axially and azimuthally and rotating in the same direction at the same speed.[32,34] Unlike the CTR system, conventional CR propellers require careful adjustment of the azimuthal phase shift between the fore and aft propellers.[33–36] This configuration originates from the idea that superimposing the sound waves generated by optimally phase-shifted blades can reduce noise emission.[34,35]

In contrast to CTR configuration, the CR motion can mitigate the BVI because of direct vortex cutting as the fore and aft propellers rotate in the same direction. The unsteady loading in a CR configuration is primarily related to the upwash and downwash generated between the propellers.[36] Despite their differences, the noise generation mechanisms of the CR configuration share several similarities with those of the CTR configuration. For instance, the aft propeller in the CR system is also subjected to the turbulence produced by the fore propeller, leading to an increase in broadband noise.[8] In terms of thrust performance, the CR configuration has received less attention than the CTR configuration.[37] It is generally expected to exhibit lower efficiency as a result of the absence of swirl recovery, although it can still outperform a single rotor of equivalent solidity when optimally configured. Through theoretical[34] and experimental[35] methods, Dobrzynski demonstrated that adding a second row of CR blades could reduce noise by 3–4 dBA in the plane of rotation with no notable performance loss. More recently, Tinney and Valdez[38] investigated the thrust and acoustic performance of a small-scale CR system using an experimental approach, demonstrating that variations in rotor speed, index angle, and axial spacing resulted in *A*-weighted sound pressure level (SPL_A) variations of up to 15 dB while maintaining similar thrust coefficients.

Further studies have confirmed the correlation between coaxial rotor operating conditions and noise mitigation. For example, McKay *et al.*[6] showed that increasing the axial spacing between the CTR propellers and clipping the aft blades can mitigate the overall sound pressure level (OSPL) while maintaining thrust. For CR propellers, Whiteside *et al.*[39] demonstrated that increasing axial spacing and decreasing azimuthal angle could increase low-frequency tonal noise but reduces broadband noise when compared to a coplanar propeller with the same number of total blades.

https://doi.org/10.1121/10.0042251

Note that existing studies mainly focus on cases in which the fore and aft rotors operate at the same speed. However, the adoption of electric propulsion now enables a broader range of tunable parameters through precise and rapid rotor-speed control. One such parameter is the differential rotor speed, i.e., the fore and aft propellers rotate at different speeds, which is expected to modify the aforementioned aero/acoustic interactions between propellers and thereby affect the acoustic–thrust performance. A recent study demonstrated the potential for noise reduction while maintaining thrust by independently adjusting the fore- and aft-propeller speeds in a CTR configuration.[40] This approach remains underexplored, particularly in CR systems, where the index angle between two propellers varies in operation.

Motivated by that, this study investigates the thrust performance and acoustic emission of a heavy-lift drone that employs differential rotor speed. The drone, developed at Delft University of Technology (TU Delft), features an octo-quad architecture and is equipped with four pairs of coaxial rotors. The fore and aft rotors operate independently and can be arranged in the CR and CTR configurations. Acoustic emissions under various conditions were recorded using a microphone arc, whereas thrust production was measured by a multicomponent balance. During the experimental campaign, the throttles of the fore and aft rotors were systematically adjusted to facilitate different combinations of rotor speeds. For different thrust levels, the corresponding SPL spectra were investigated to uncover the link between differential rotor speeds and noise characteristics when considering human hearing.[41] Comparisons of the acoustic and thrust performances are made between the CR and CTR configurations. The findings of this study are interpreted to foster discussion and provide insights into the underlying aerodynamic and aeroacoustic mechanisms of coaxial rotor systems. Moreover, the results can offer guidance for optimizing thrust and acoustic performance in coaxial UAVs by introducing differential rotor-speed control as a novel operational parameter.

The remainder of the paper is organized as follows. Section II describes the methodology of this study, including details on the experimental setup, whereas Sec. III discusses the relation between differential rotor speeds, noise level, and thrust production, followed by evaluation SPL spectra under various operating scenarios.

II. METHODOLOGY

A. Multicopter drone

In this study, the noise emission and thrust performance of an octo-quad multirotor UAV developed at TU Delft were investigated, as shown in Fig. 1. The UAV is categorized as a compact-heavy-lift drone and is capable of carrying a payload of around 5 kg with a maximum takeoff mass of 24 kg. As depicted in Fig. 2, the drone has a square footprint of 854 mm × 854 mm and a height of 307 mm. Its internal frame is machined from a single piece of aluminum and equipped with four pairs of coaxial rotors, each enclosed within a protective propeller guard as displayed in Fig. 2(b). The propeller guard was constructed from carbon-fiber-reinforced plastic to protect surrounding personnel and property from potential collisions and flying debris. The presence of guards interferes with the flow field induced by the operating propellers, contributing to the overall installation effect.

Based on performance and geometry considerations, the top (fore) rotors use four-bladed APC 14 × 7E propellers (Woodland, CA). The bottom (aft) rotors are also equipped with four-bladed APC 15 × 10E propellers. The aft blades are set at a slightly higher pitch angle than the fore blades to compensate for the reduction in effective angle of attack caused by accelerated inflow.[13,36,42] The fore and aft propellers feature an axial spacing of 176 mm, which corresponds to approximately 0.48D. Here, D (368 mm) is defined as the mean of the fore (14-in.) and aft (15-in.) propeller diameters. Details on the selected propellers are documented in our previous study[40] and University of Illinois at Urbana–Champaign propeller database.[43,44] The UAV's propulsion system is based on T-Motor (Nanchang, People's Republic of China) AT4130 450KV brushless direct-current (DC) motors, where each has a maximum power output of 1.8 kW. Motor speed is regulated by T-Motor T60A electronic speed controllers, which control the throttle using pulse-width modulation signals at an update rate of 400 Hz. The propulsion system permits independent control of the fore and aft rotor groups, allowing differential speed adjustments between the coaxial propellers. Additionally, the propellers can be configured in a CR or CTR arrangement by adjusting the mounted blades. The propeller blades in the CR configuration are mounted in the same rotational direction, whereas the CTR configuration replaces the aft-propeller blades with those that reverse leading and trailing edges. The system does not allow for controlling the index phase between rotors. Thus, it is important to stress that the results for the CR configuration do not include conditions in which the revolutions per minute (RPM) for both rotors are identical. Minor variations in RPM are expected even when

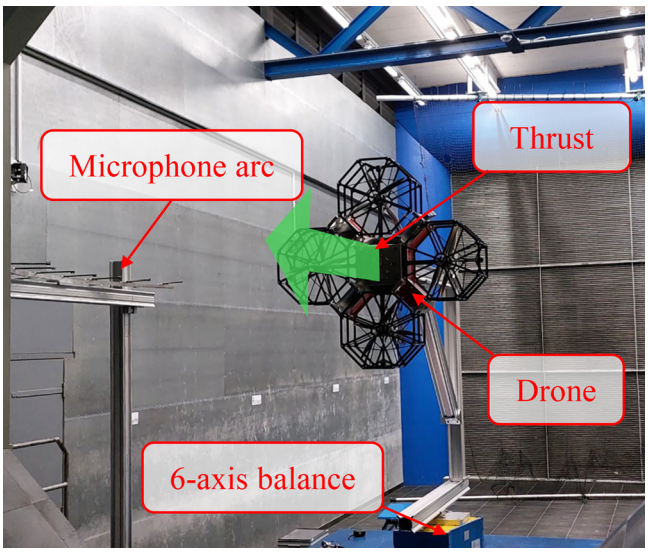

FIG. 1. Illustration of experimental setup with the external balance, microphone arc, drone, and thrust direction annotated.

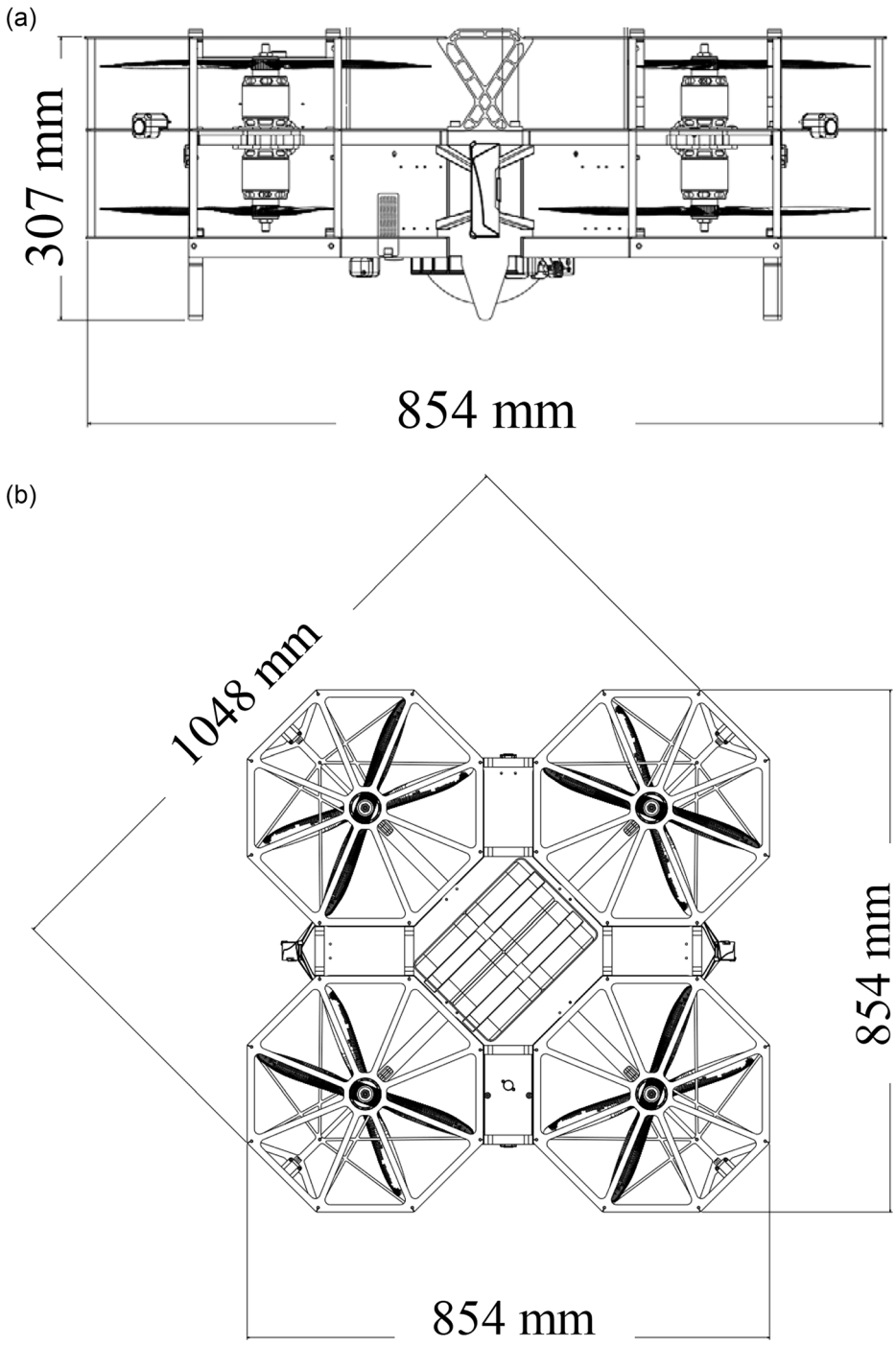

FIG. 2. Drawings of the octo-quad UAV show the (a) side view and (b) top view. The tested model has four blades on each propeller.

the propellers are controlled with identical throttle settings. In addition, this configuration tends to reinforce the swirling motion in the wake, which can reduce the thrust production of the aft propellers.[36] To maintain stable operation in high-throttle settings, the drone is powered by four lithium-polymer batteries (GensTattu 6S, Livermore, CA), each of which has a capacity of 12 000 mA h and operates at an average nominal voltage of 22.2 V with a discharge rate of 30C. During operation, the motors draw a continuous current of ∼17 A, resulting in an approximate testing time of up to 21 min for a 50% discharge.

B. Facility and measurement techniques

The drone is tested in the open jet facility (OJF) of TU Delft. The facility flow in the chamber that can be used is 3 m × 3 m × 6 m in dimension, and its side walls are covered with perforated panels to absorb acoustic waves. Despite the latter, the facility is not meant to create an anechoic environment, and reflections are to be expected. As depicted by the thrust direction in Fig. 1, the drone is placed facing the wind tunnel nozzle to avoid recirculation effects, and thrust measurements were performed through a six-axis balance system, which is attached to the drone.

https://doi.org/10.1121/10.0042251

As illustrated in Fig. 1, acoustic measurements are performed with a directivity arc composed of seven microphones placed along the vertical axis describing a semicircle from −30 to 30 deg, in 10 deg steps. G.R.A.S. 46BE microphones (Holte, Denmark), characterized by a flat frequency response from 10 to 40 kHz (±1 dB), are used. The acquisition of each condition is taken for 10 s at a sampling rate of 51 200 Hz and controlled with an NI cDAQ system (Austin, TX) equipped with NI-9234 boards. To improve the statistical convergence of the SPL spectra analysis, each acoustic measurement is divided into 0.64-s segments with 50% overlap.[45] The segmentation yields a total of 30 segments and a frequency resolution of 1.6 Hz, ensuring convergence and accurate detection of tonal noise. The RPM of the rotors are controlled with an NI 9401, which has individual controls for the fore and aft motors.

III. RESULTS AND DISCUSSION

In this section, the thrust performance and noise emissions of the drone under steady conditions with zero inflow (an advance ratio of zero) are analyzed and discussed. The investigation is conducted for the CR and CTR configurations and consists of evaluating the performance-acoustics trade-offs and noise spectra analysis. The former is investigated by analyzing noise levels against load factor, whereas the latter is examined through noise spectral analysis. Here, the load factor is defined as the thrust-to-weight ratio of the propeller set, and the drone hovers at a load factor of ∼1 when all propellers operate at approximately 70% and 60% throttle for the CR and CTR configurations, respectively. Note that the noise results are derived from the microphone placed at the drone's hovering height within the symmetry plane between two coaxial propellers. At this directivity angle, tonal noise is expected to exhibit a more distinguishable power level than broadband noise.[46] The rotor-speed combinations in the subsequent context are presented in the form of (Ω_{fore}, Ω_{aft}), where Ω_{fore} and Ω_{aft} denote the fore and aft rotor speeds in RPM, respectively.

First, the potential of employing differential rotor speed to optimize the acoustic–thrust performance in CR and CTR configurations is assessed by analyzing noise variation across different rotor-speed combinations and load factors. As illustrated in Fig. 3(a), for the CR arrangement, the general level of the *A*-weighted overall sound pressure level (OSPL_A) within the noise envelope exhibits an expected increase with increasing load factor and correlates with the fore and aft rotor speeds. For instance, the actuation RPM required to produce a minimum load factor of 0.05 is (0,1780), whereas a maximum load factor of 1.42 is attained

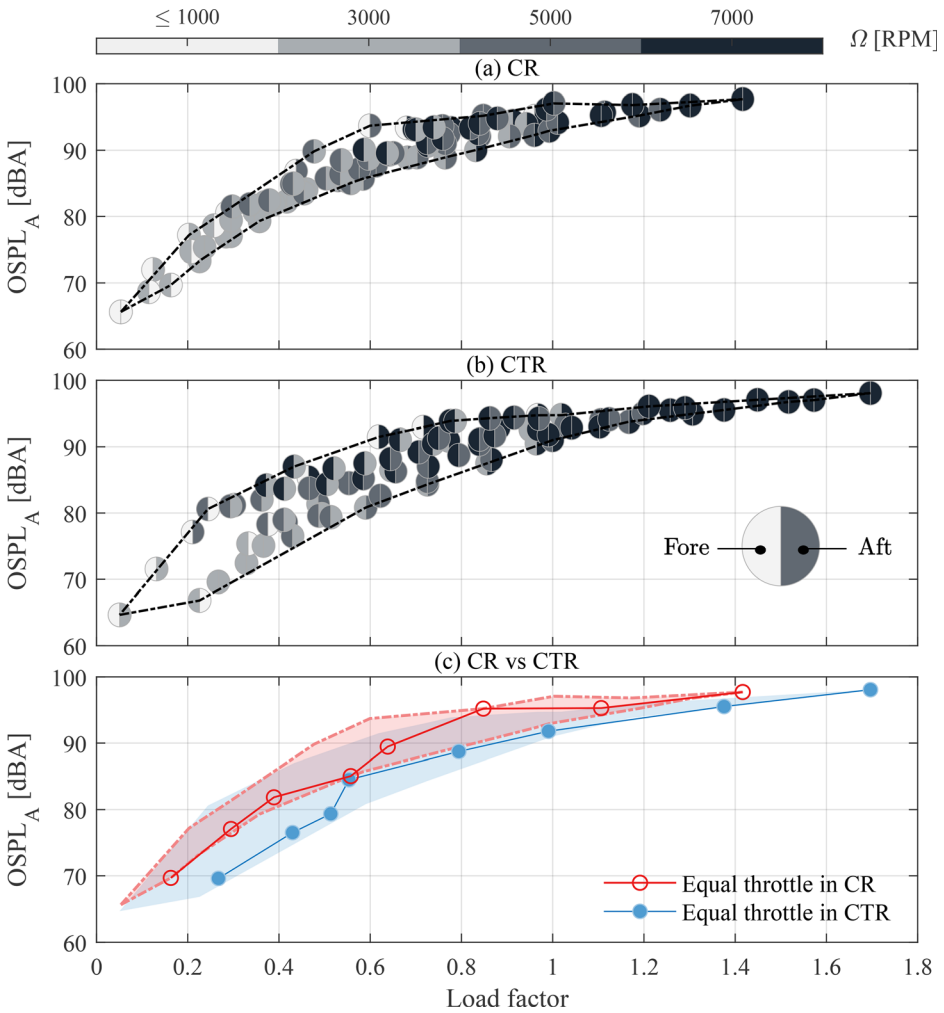

FIG. 3. Plots of OSPL_A against load factor for (a) CR and (b) CTR propellers with differential rotating speeds and (c) a comparison between the two. The shaded circles represent a rotor-speed combination, where the left and right halves indicate the RPM of the fore and aft rotors. In (a) and (b), dotted-dashed lines denote the trends of local max and min OSPL_A under different loading conditions. The noise envelopes produced by the CR and CTR configurations are presented in transparent red (with dotted-dashed-line edge) and blue (no edge), respectively. The overlaid solid lines represent the equal-throttle operation. Note that the CR and CTR configurations are denoted by empty and solid circles, respectively.

by spinning the rotors at a speed of (6700,6840) with both rotors operating at 80% throttle. The noise envelope pattern further suggests that adjusting the rotor-speed combination could induce a noise variation for the same thrust. Regarding the local maximum noise level, a notable increase in $OSPL_A = 28.1$ dBA is observed as the load factor rises, particularly for values below ~ 0.6. Interestingly, a further increase in load factor up to 1.42 results in a noise penalty of only ~ 4 dBA. This observation could be attributed to the noise scaling with respect to the rotor speeds and will be further discussed in the subsequent context.

Consistently with the CR configuration, Fig. 3(b) shows that the CTR arrangement also exhibits an increase in local maximum and minimum noise with increasing load factor and rotor speeds. The actuation RPM of (0,1850) produces a minimum load factor of 0.05, which is similar to that observed in the CR configuration. Here, similar thrust performance is anticipated between the two configurations, as no swirl recovery takes place when the fore propeller is held at zero throttle. The system is effectively single rotor in this condition. On the other hand, the maximum load factor ($\sim$1.70), despite being generated under the same throttle input (80%,80%), is approximately 0.28 higher than that of the CR arrangement at the cost of a $\sim$0.4 dBA rise in $OSPL_A$. The improvement in load factor can be attributed to the swirl recovery as a result of the CTR motion, whereas the minor increase in $OSPL_A$ suggests that the noise levels are primarily influenced by the rotor speeds. A steep increase in local maximum noise is observed mainly at load factors below 0.24 as the aerodynamic loading is carried primarily by the aft propellers alone. In contrast, the increase in local minimum noise is much less pronounced across all load factors. For the CR and CTR configurations, local maximum noise trends include several rotor-speed combinations in which the fore propeller remains uncontrolled with zero throttle input. As shown in Fig. 3, all of these combinations are observed at load factors between 0.6 and 0.8.

A comparison of the noise envelopes for the CR and CTR configurations is presented in Fig. 3(c). Here, the equal-throttle condition refers to the fore and aft rotors receiving the same throttle input, representing the conventional operating mode for coaxial propellers. The ranges of $OSPL_A$ for the CR and CTR configurations are observed to be from 69.7 to 97.7 dBA and from 69.6 to 98.1 dBA, respectively. For the same noise level, the CTR configuration is observed to achieve a load factor of at least 0.1 higher than that for the CR configuration. For the same load factor, the CTR radiates up to 8 dBA less noise compared to the CR. The local minimum noise in the CR configuration is primarily generated by equal-throttle operation, except within the load factor range of 0.56–1.11. A similar trend is observed for the CTR configuration, with the exception occurring between load factors of 0.51 and 1.00. The finding that the CR configuration generally produces higher noise levels than the CTR configuration at the same load factor can be attributed to two elements. First, there is the absence of azimuthal phase shift optimization between the fore and aft propellers;[33–36] and second, the higher aerodynamic efficiency of the CTR rotors resulting from swirl recovery allows the propellers to operate at lower RPM compared to the CR configuration for the same thrust output. In addition, for the configurations explored in this study, the transparent blue envelope (no edge) exhibits a greater vertical span than the red envelope (with edge), indicating that the noise variation in the CTR configuration is more pronounced compared to that in the CR configuration. The larger noise variation observed in the CTR configuration may be attributed to the greater relative rotor speed, which amplifies the effects of wake interactions. In contrast, the propellers in the CR configuration experience weaker relative motion and interaction between the propellers as both propellers rotate in the same direction. This observation underscores the importance of controlling the differential rotor speed to minimize noise penalties.

To better visualize the acoustic–thrust differences between the CR and CTR configurations, performance–noise contours are illustrated in Fig. 4. The contours are computed from irregularly scattered measurement data using cubic interpolation and only consider nonzero differential rotor speeds. Note that Fig. 4 is intended as a general guide for reflecting the overall trends rather than providing precise quantitative predictions. The performance–noise contour of the CR configuration is presented in Fig. 4(a) as a reference, whereas Fig. 4(b) illustrates the corresponding load factor difference (Δ load factor) and noise ratio ($\Delta OSPL_A$) between the CR and CTR configurations (CR − CTR) over a grid of matching RPMs. As observed in Fig. 4(a), the load factor increases more with increasing Ω_{aft}. This is consistent with the design choice, where the thrust–RPM gradient of the aft propeller is expected to be larger than that of the fore propeller because of its higher pitch angle. In addition to that, the particle image velocimetry results from De Gregorio *et al.*[47] on a CTR propeller showed that the slipstream from the fore propeller can disrupt the performance of the aft propeller, leading to a reduction in thrust output and an increase in torque demand, thereby compromising the overall load factor. Furthermore, as a result of the presence of motors and frame structure downstream of the fore propellers, the aft propellers may produce a cleaner slipstream with greater induced velocity and momentum compared to the fore propellers.[47] However, this point warrants further investigation, particularly to examine the influence of the propeller guard on the characteristics of the aft-propeller slipstream. Nevertheless, it is observed that the CR configuration produces notable smaller thrust ($-0.3 < \Delta$load factor < -0.1) than the CTR configuration across the grid of RPM. The CTR configuration, despite this thrust advantage, does not incur a noise penalty for most matching RPM settings, with the exception of the region near (4000,6500). A quick inspection on the unweighted results suggests that *A*-weighting filter does not alter the contour of $\Delta OSPL_A$ notably, apart from the vicinity of (5600,5400), where $\Delta OSPL_A$ is nearly zero.

To assess the acoustic differences between differential rotor speed and conventional operating modes, Fig. 5

https://doi.org/10.1121/10.0042251

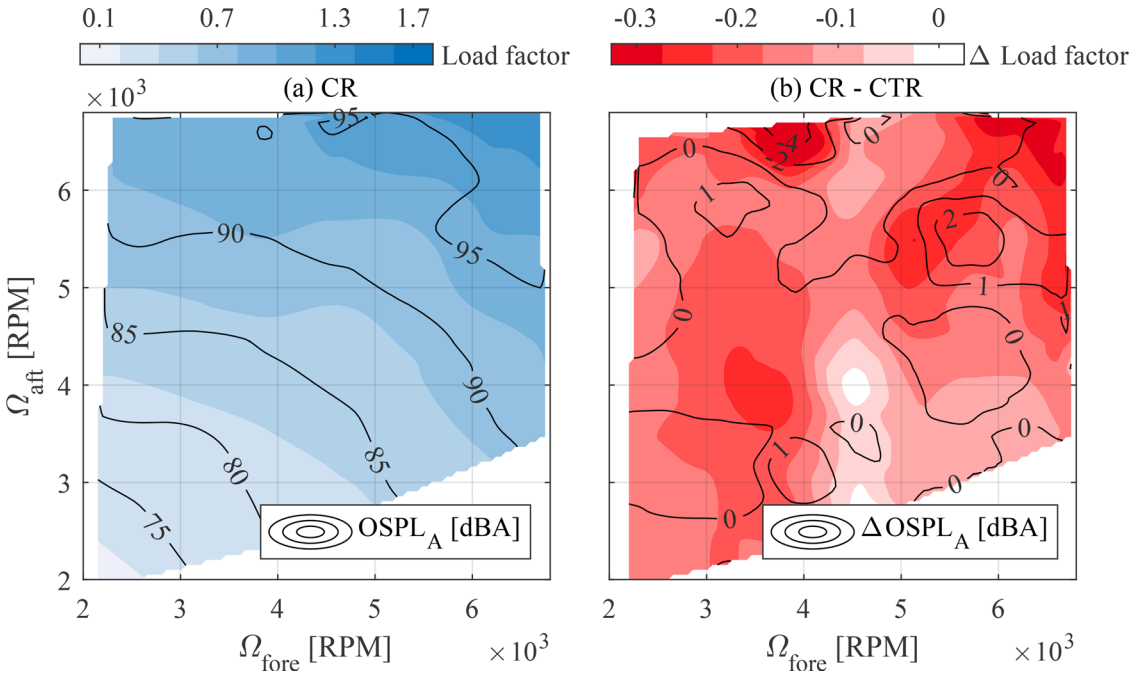

FIG. 4. Performance–noise contours of propellers in the (a) CR and (b) CR − CTR configurations. The levels of $OSPL_A$ and $\Delta OSPL_A$ are illustrated using black-line contours, whereas load factor and Δ load factor are presented in blue (left) and red (right) contours, respectively.

presents a comparison of their OSPLs under equivalent load factors, where the *A*-weighting effect is also illustrated. For reference, the equal-throttle results are shown in Figs. 5(a) and 5(b) for the CR and CTR arrangements, respectively. The evaluation of the equal-throttle setting based on Figs. 5(a) and 5(b) indicates that the RPM of the fore and aft rotors aligns well across most load factors for both configurations. The fore propellers are observed to rotate slightly faster than the aft propeller with a difference below 400 RPM, which may be attributed to a smaller pitch angle compared to that for the aft blades. The relatively larger difference in RPM at low throttle settings is likely due to the fact that the rotors are more susceptible to flow interactions between the propellers. The *A*-weighting noise-reduction effect, depicted by the dashed line, gradually diminishes with increasing load factor as the first BPF shifts toward a higher frequency range, where the *A*-weighting attenuation effect becomes weaker. By comparing the solid and dashed black lines in Fig. 5, the maximum noise variation caused by *A*-weighting filter (ΔOSPL) is observed to be 3 dB when the drone operates in the CR configuration with a minimum load factor of 0.16. Apart from that, the *A*-weighting–induced ΔOSPL for most tested differential rotor-speed combinations remains around or below 1 dB, regardless of whether the rotors operate in the CR or CTR configuration. Hence, the subsequent discussion focuses primarily on the *A*-weighted results for brevity.

As shown in Figs. 5(c)–5(f), deviating from the conventional equal-throttle operation enables noise reduction but may also result in increased noise as most of the investigated rotor-speed combinations increase noise from the equal-throttle condition. Note that most of the high- and low-noise results are derived based on the local maximum and minimum $OSPL_A$ from Fig. 3. For the high-noise plots in Figs. 5(c) and 5(d), cases in which the fore rotor has zero throttle input ($\Omega_{fore} = 0$) are highlighted in red (light gray) to distinguish them from the others as their high-noise emission is primarily associated with a single high-RPM rotor rather than differential rotor speed. The rotor-speed combinations that yield the second-highest $OSPL_A$ for a given load factor are selected to estimate $\Delta OSPL_A$ and ΔOSPL. Because the available measurements do not correspond to the exact same load factors for equal-throttle, high-noise, and low-noise conditions, the values of $\Delta OSPL_A$ and ΔOSPL are obtained from linearly interpolated noise measurements.

On inspecting the difference in fore and aft rotor speeds in, respectively, Figs. 5(c) and 5(d) for a given load factor below 0.9, it is observed that the fore rotor needs to rotate much faster than the aft rotor, i.e., on the order of 1000 RPM, compared to the equal-throttle setting. An outlier occurs in Fig. 5(d) at a load factor of 1.02, where the aft propeller operates at 80% throttle while the fore propeller remains at only 10%, nearing an uncontrolled state. To achieve a load factor greater than one, the aft propellers must increase their rotating speed, resulting in a smaller differential rotor speed and less $OSPL_A$ variation compared to the equal-throttle operations. The observation suggests that rotating the fore propellers faster than the aft propellers should be avoided for this drone as it leads to higher noise. As previously noted, this phenomenon can be associated with the aerodynamic characteristics of the propellers. Achieving a desired load factor by increasing the fore-propeller thrust may require a substantial increase in Ω_{fore},

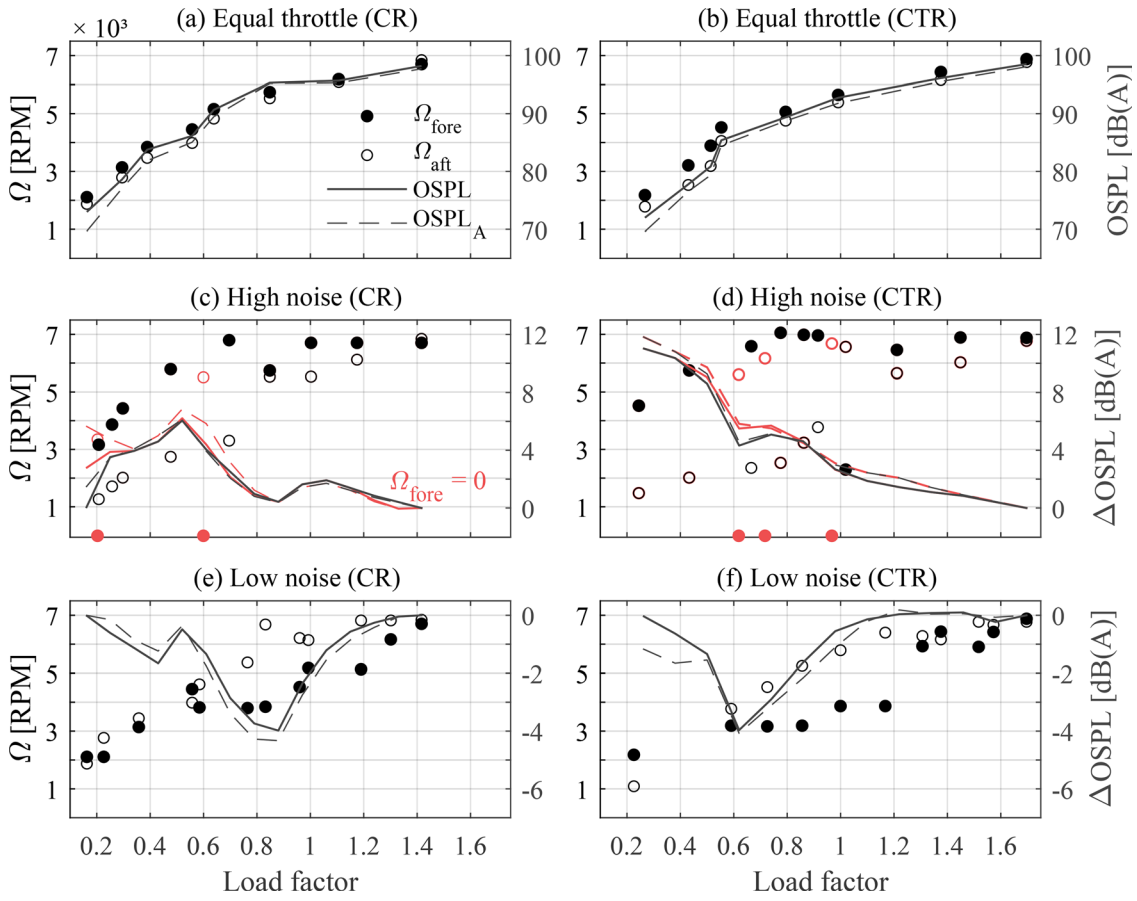

FIG. 5. Trends of Ω and minimum OSPL/$OSPL_A$ with increasing load factor for CR propellers in (a), (c), and (e) and CTR propellers in (b), (d), and (f) are displayed. The left axis indicates the scale of Ω, whereas the right axis represents the noise level. The Ω values for the fore and aft propellers are represented by solid and empty circles, whereas OSPL and $OSPL_A$ are shown with solid and dashed lines, respectively. Groups of subplots (a) and (b), (c) and (d), and (e) and (f) correspond to conditions of equal-throttle, high-, and low-noise conditions, respectively. In (c) and (d), cases in which $\Omega_{fore} = 0$ are depicted in red (light gray).

leading to elevated rotational noise caused by the associated increases in thrust and torque.[48,49] Moreover, a faster-rotating fore propeller can lead to more severe turbulence ingestion for the aft propeller because the turbulence intensity in the rotor wake is proportional to the rotor speed.[50] In addition, the large increase in RPM reduces the noise attenuation effect under *A*-weighting. It is also worth noting that the fore propellers in the CR and CTR configurations maintain a relatively constant speed between 6000 and 7000 RPM at load factors above approximately 0.6. As propeller noise typically scales with tip speed as U^n, where n depends on the noise source,[51] a relative constant Ω_{fore} suggests that the increasing load factor introduces little noise penalty. Furthermore, because thrust is generally proportional to U^2, a modest increase in rotor speed can lead to a substantial rise in thrust.[52] This relation helps to explain the significant performance improvement as Ω_{aft} gradually approaches Ω_{fore}. Enhanced aerodynamic efficiency may also contribute to this trend, whereas further investigation of the flow field with propeller–propeller interaction is required.

The results of low-noise scenarios are then presented in Figs. 5(e) and 5(f), and the impact of differential rotor speeds on noise reduction is examined. For the CR and CTR configurations, it appears that spinning the aft propeller faster than the fore propeller could reduce the emitted $OSPL_A$ when the UAV is moderately loaded (between load factors of 0.6 and 0.9). Such an observation can be attributed to several hypotheses that may mitigate the unsteady loading within the system. First, the aft propeller, which operates at a higher pitch angle, has a higher static thrust-to-RPM ratio. Increasing its rotational speed can reduce the adverse impact of the nonzero inflow on the effective angle of attack and is more effective in reducing the overall propeller loading. Second, spinning the aft propeller faster than the fore propeller can increase the induction velocity, thereby mitigating the BVI in the rotational plane of the fore propellers.[21,36] According to Hong *et al.*,[21] the miss distance (axial direction) between a blade and the tip vortex shed by the preceding blade is inversely proportional to the stacking distance in a coaxial system. With an axial spacing of 0.5*D*, the miss distance increases by 10% when compared to a single rotor configuration.[21] It is observed in Fig. 5(e) that the reduction in $OSPL_A$ correlates with the magnitude of the differential rotor speeds, particularly, between load factors of 0.58 and 1.13. However, for the CTR configuration, this trend is not evident, and further flow-field measurements can help clarify the trend.

https://doi.org/10.1121/10.0042251

Subsequent analysis of the noise spectrum is conducted to examine how differential rotor speeds influence noise emissions in the frequency domain, in particular to the influence on noise elevation and reduction while maintaining the same thrust. It is worth reiterating that the analysis is based on microphone measurements taken at the hovering height, where tonal peaks are expected to be more distinguishable from broadband noise.[46] Additional inspections using microphones at other locations confirm that the overall spectrum pattern remains consistent, regardless of variations in directivity angle.

The noise spectra associated with the CR configuration at load factors of approximately 1.42, 0.84, and 0.27 are presented in Figs. 6(a), 6(b), and 6(c), respectively. These load factors refer to high-, medium-, and low-loading conditions. The spectra are plotted up to 5 kHz, covering the most critical hearing-sensitive range. It is important to note that for these conditions, most of the exact load factors differ from the indicated values within a range of ±9%. The load factor for the low-noise condition at a load factor of ∼0.27 deviates more significantly than the rest, which is approximately 17% lower than the indicated value. These discrepancies arise from the availability of measured thrust as the experiments were conducted by systematically varying the throttle input, which did not translate equally to the load factor.

As displayed in Fig. 6(a), the maximum thrust of the drone in the CR arrangement is achieved when the fore and aft propellers operate at the maximum tested throttle with a rotor-speed combination of (6703,6844) RPM and an $OSPL_A$ of 97.7 dBA. This high load factor is attainable only through equal-throttle operation and, thus, no spectra corresponding to high- and low-noise conditions are presented. Additionally, the SPL spectrum, with an OSPL of 98.2 dB, is plotted to illustrate the *A*-weighting effect. As expected, the spectra of SPL and SPL_A exhibit nearly identical trends. The slight reduction (0.5 dB) in the overall noise level caused by *A*-weighting is primarily attributed to the attenuation of spectral components below 1 kHz. The *A*-weighting filter also elevates the acoustic energy of spectral components above 1 kHz, where this penalty becomes increasingly significant at higher rotational speed. The *A*-weighted noise spectrum shows that the most powerful tonal peaks for both propellers, highlighted by vertical lines, reside at around 900 Hz, corresponding to the second harmonics. Because both propellers rotate at similar RPM, their BPF tones form a distinct fork-shape peak. The first BPF tones, which typically exhibit the dominant spectral peak, are attenuated by the *A*-weighting effect but still produce SPL_A peaks that are comparable to the second BPF peaks. Three pairs of fork-shaped peaks are observed between the BPF tones. This is attributed to the noise induced by shaft rotation as they occur at frequencies of the integer multiples of ∼110 Hz defined by $\Omega/60$. Beyond the second harmonics, the shaft tones appear to make a notable contribution to the overall noise along with the broadband noise.

In the medium-load scenario (∼0.84), only the noise spectra corresponding to high- and low-noise operations are presented in Fig. 6(b) as a result of measurement availability. In this case, the high-noise condition corresponds to the equal-throttle operation, where the dominant spectral peak is observed at 732 Hz, produced by the aft propeller's second harmonics. The second BPF tone of the fore propeller occurs close to that of the aft propeller, forming a characteristic multifrequency tone. However, unlike the well-separated double-peak structure observed under high load conditions in Fig. 6(a), the multifrequency peak here appears as a cluster of several narrow peaks, likely resulting from the superposition of tonal noise generated by different sources. The two dominant peaks are associated with the BPF tones as the fore and aft propellers operate at similar RPM. The weaker peaks may be attributed to haystacking near multiples of the aft-propeller BPF tones, originating from the aft propellers cut through wake induced by the fore propellers. More specifically, this spectral broadening can be associated with loading correlations of successive blades caused by turbulence ingestion.[51,53,54] Similar spectral peaks have been observed in previous studies when propellers operate in distorted inflow conditions.[53,55–58] Consistent with the observation in Fig. 6(a), groups of multifrequency peaks are noticed at integer multiples of approximately 95 Hz and are attributed to shaft noise because of motor imbalance. Inspecting low-noise operation, a reduction in $OSPL_A$ of 5.2 dBA is observed by reducing the fore rotor speed by ∼2000 RPM and increasing the aft rotor speed by ∼1000 RPM with respect to the equal-throttle condition. As expected, the spectral peak corresponding to the second BPF is further separated compared to equal-throttle operation as the differential rotor speed is larger (∼2000 RPM), and the most pronounced peak is produced by the aft propeller. With differential rotor speed, reductions in tonal amplitude and broadband noise level are observed relative to the equal-throttle case, suggesting a possible decrease in overall propeller loading as well as mitigated turbulence ingestion.

The noise spectra corresponding to a load factor of approximately 0.27 are presented in Fig. 6(c). Under equal-throttle operation, the UAV emits an $OSPL_A$ of 77.1 dBA. The BPF tones generated by the fore propeller exhibit comparable SPL_A levels (ranging approximately between 50 and 54 dBA across the first several harmonics) despite the influence of *A*-weighting. These tones still exhibit a fork-shaped spectral pattern, although the fork teeth do not align with the BPFs of the adjacent aft propeller. The observation is likely the result of complex flow interactions between the rotors, which is similar to the multifrequency peaks observed in Fig. 6(b). Nonetheless, the scattering of tonal energy over a wider frequency band complicates the evaluation of the relative importance of the noise sources.[54] Shaft noise remains present, appearing at integer multiples near 50 Hz. By increasing the rotational speed of the fore propeller, $OSPL_A$ increases by 4.4 dBA, reaching the high-noise condition. The spectral pattern of the dominant fore-propeller tones resembles that of the equal-throttle condition, exhibiting double-peak pattern, despite the RPM of the fore and aft rotors being different by ∼2400 RPM. This might be related

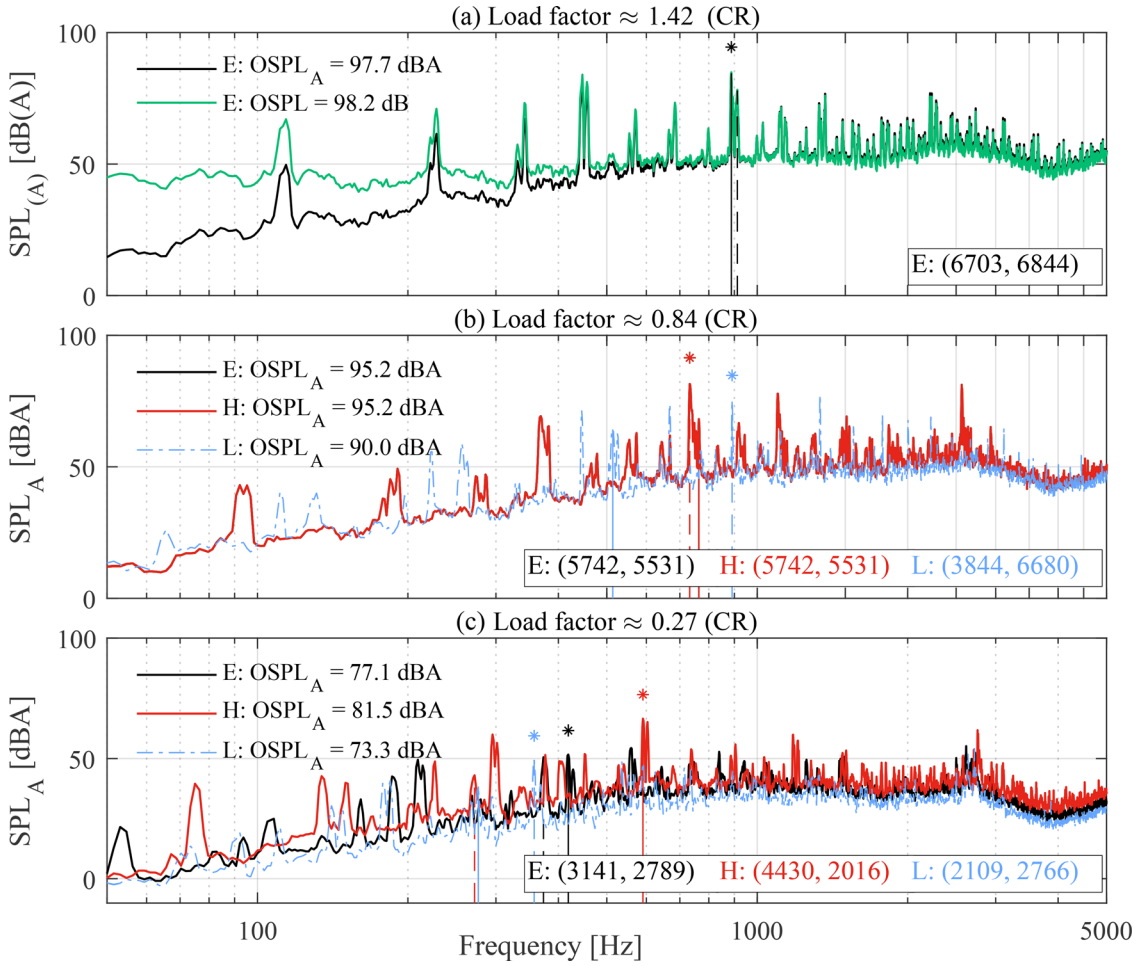

FIG. 6. Spectra of $SPL_{(A)}$ at load factors of (a) 1.42, (b) 0.84, and (c) 0.27. The content corresponding to equal-throttle (E), high-noise (H), and low-noise (L) conditions are represented in black, red (dark gray) lines, and blue (light gray) dotted-dashed line, respectively. The associated $OSPL_{(A)}$ and rotor-speed combinations in RPM are annotated, following the same color code. The second BPF tones for the fore and aft rotors are highlighted using vertical solid lines and dashed lines, where the dominant SPL_A in the rotor pair is marked by an asterisk. For the case with load factor of 1.42, the SPL is plotted alongside SPL_A to demonstrate the effect of *A*-weighting filter on noise spectrum.

to the quasiperiodic nature of rotor speed, given that the aft motor speed is close to half that of the fore motor, and aerodynamic interaction plays a role. In contrast to the equal-throttle operation, the BPF tones produced by the aft propeller under the low-noise condition are less distinguishable from the broadband noise. A reduction in $OSPL_A$ by 3.8 dBA is achieved by operating the aft propeller more than the fore propeller. Under this condition, the second BPF of the aft propeller appears as the most powerful tone, whereas the difference in SPL_A between tonal and broadband components is near negligible beyond third harmonics. Overall, the tonal and broadband noise are lower than those observed in the equal-throttle operation, suggesting that the loading on all propellers and turbulent wake might be less intense than the equal-throttle condition.

Subsequently, a similar spectral analysis is performed for the CTR configuration, and the noise spectra corresponding to load factors close to 1.38, 0.77, and 0.25 are presented in Figs. 7(a), 7(b), and 7(c), respectively. The load factors are carefully selected with the aim of matching those presented in Fig. 6. Under high loading conditions, the major spectral peaks shown in Fig. 7(a) are primarily associated with the second BPF of the propellers and appear in the frequency range of 800–900 Hz. Similar to the result of the CR configuration, the SPL_A levels corresponding to first BPF tones (near 400 Hz) are comparable to those of the second BPF despite the attenuation imposed by the *A*-weighting process. It is interesting to note that the SPL_A levels associated with broadband noise remain similar across all operating conditions. In contrast, the tonal peaks related to shaft noise, most obvious at 115 and 230 Hz, appear to follow the same rank as $OSPL_A$, suggesting that these tones may be the main contributors to the observed variation of 2.2 dBA in $OSPL_A$ as a result of differential rotor speed. The variation is expected to be small, as the fore and aft propellers must operate near maximum throttle to achieve a high load factor, limiting the degree of differential rotor-speed adjustment and its impact on noise characteristics.

For the medium-load condition displayed in Fig. 7(b), the equal-throttle operation results in an $OSPL_A$ of 88.7 dBA. The corresponding noise spectrum reveals that the second BPF tones, located near 700 Hz, exhibit the

https://doi.org/10.1121/10.0042251

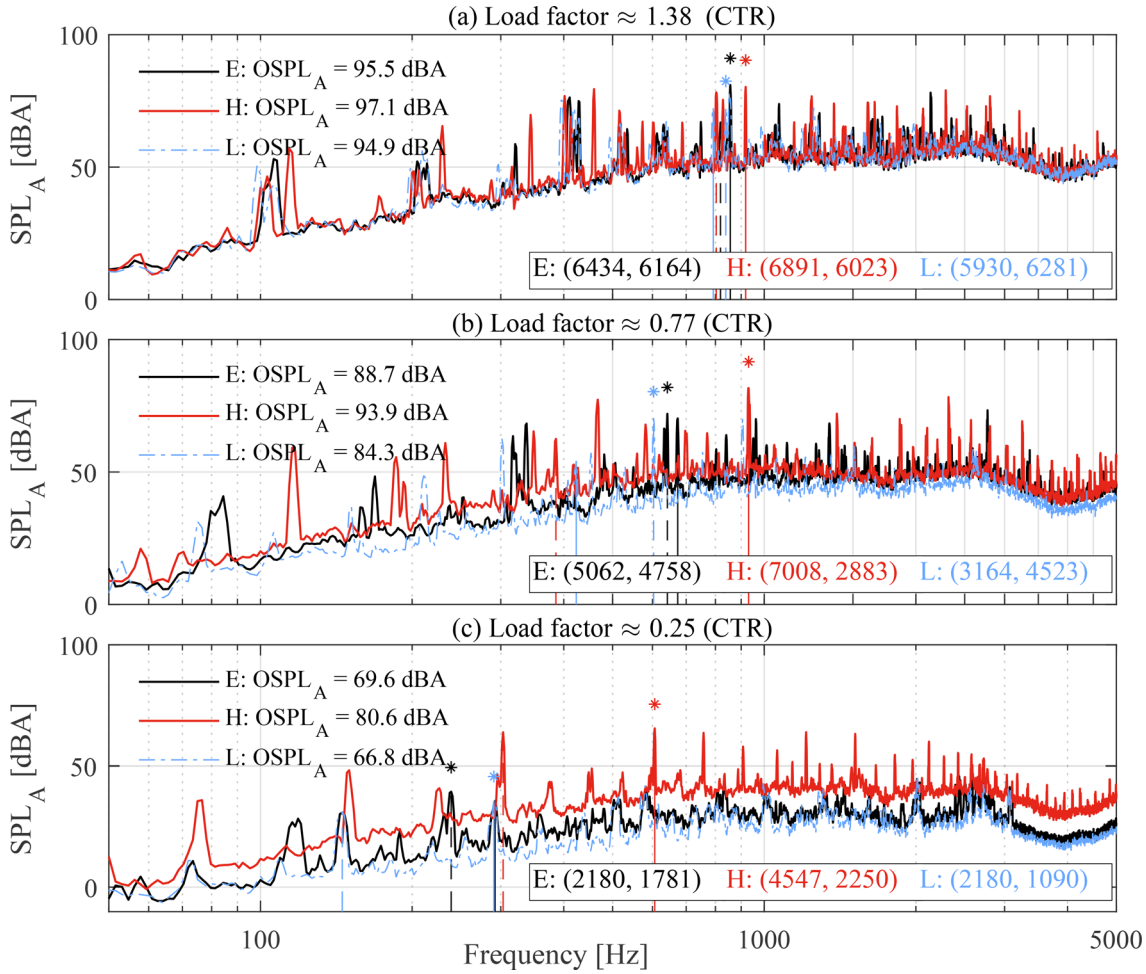

FIG. 7. Spectra of SPL_A at load factors of (a) 1.38, (b) 0.77, and (c) 0.25. The content corresponding to equal-throttle (E), high-noise (H), and low-noise (L) conditions are represented in black, red (dark gray) lines, and blue (light gray) dotted-dashed line, respectively. The associated $OSPL_A$ and rotor-speed combinations in RPM are annotated, following the same color code. The second BPF tones for the fore and aft rotors are highlighted using vertical solid lines and dashed lines, where the dominant SPL_A in the rotor pair is marked by an asterisk.

strongest spectral peaks, where the dominant tone is generated by the aft propeller. By significantly increasing the loading on the fore propeller, $OSPL_A$ increases by 5.2 dBA compared to the equal-throttle operation, and the fore propeller generates a much stronger BPF tone than the aft propeller as highlighted by the vertical solid and dashed lines for the second harmonics. Additionally, the fore shaft noise emits strong tonal peaks at integer multiples of 117 Hz. The tonal components are generally higher than those observed under equal-throttle conditions, particularly above 1 kHz, where hearing sensitivity is high. This is attributed to the joint effects of the *A*-weighting filter and the unsteady loading that scales with RPM. As expected, the low-noise condition is produced by spinning the aft propeller faster than the fore propeller, which leads to a 4.4 dBA reduction in $OSPL_A$ compared to the equal-throttle condition. Despite the dominant spectral peaks of the first three harmonics exhibiting similar SPL_A levels compared to their counterparts under the equal-throttle condition, the tonal and broadband noise components above 1 kHz appear at a lower SPL_A than those observed in the equal-throttle case.

At a load factor close to 0.25, the noise spectrum of the high-noise condition exhibits a significantly higher $OSPL_A$ of 80.6 dBA compared to the equal-throttle (69.6 dBA) and low-noise (66.8 dBA) conditions, owing to the substantially elevated SPL_A levels of the tonal and broadband components observed in Fig. 7(c). Compared to the CR configuration shown in Fig. 6(c), the spectral peak energy in the CTR configuration appears more concentrated in the frequency domain (clear peaks) despite having similar differential rotor speeds, i.e., (4430,2016) in CR vs (4547,2250) in CTR. This suggests that CTR motion produces more periodic propeller–propeller interaction than the CR motion for a similar differential rotor speed. For the equal-throttle and low-noise conditions, the dominant spectral peaks are associated with the second harmonics (highlighted by vertical lines), and no distinct spectral peaks are observed at higher frequencies. This pattern is similar to that observed in Fig. 6(c) for the CR configuration.

After assessing the CR and CTR configurations, one interesting observation is that most cases in which the fore propellers rotate faster than the aft propellers exhibit some

extent of haystacking. Because the turbulence level in rotor wake is proportional to the rotor speed,[50] the observation is likely caused by the fore propellers generating a more turbulent slipstream, which is ingested by the aft propellers. When compared with the spectral results of McKay *et al.*,[6] which also examines a CTR propeller at hovering height, the present results do not exhibit strong interaction tones whose amplitudes are comparable to or even greater than the BPF tones at high frequencies. This may be due to the limited BVI tonal noise resulting from the relatively large spacing between the propellers ($0.48D$) compared with conventional configurations ($<0.25D$).[6,39,59] The increased spacing can weaken propeller–propeller interactions[60,61] as the vortex structures shed by the fore propeller travel a greater distance and diffuse more before reaching the aft propeller. In addition, the BVI occurring in the vicinity of the aft propeller can also shift inboard, where the sectional blade speed and thrust can be lower as the fore-propeller wake contracts.[14] Additional flow-field measurements would help clarify the observation.

IV. CONCLUSION

An experimental study is conducted to investigate differential rotor speed as a novel operating parameter for improving multicopter thrust and noise performance. The investigated drone is equipped with four groups of coaxial rotors, each consisting of a fore and aft propeller with an axial spacing of about $0.48D$. Each propeller group can be configured in either CR or CTR arrangements and operate with differential rotor speeds. The experimental campaign is performed in an OJF, where the UAV's acoustic emissions and thrust output are measured under steady operating conditions with zero inflow. During the campaign, the throttle inputs of the fore and aft propellers are systematically increased to enable various rotor-speed combinations under the CR and CTR configurations. Analyses on the relation between different rotor-speed combinations, load factors, and noise level are performed.

The results demonstrate that the same thrust can be achieved through different rotor-speed combinations for the CR and CTR configurations. The maximum load factor, based on the drone's operational weight, achieved by the CTR configuration is 1.70, which is 0.28 higher than that obtained with the CR configuration (1.42). Under equal-throttle conditions, the CTR configuration generally produces more thrust than the CR arrangement with the same throttle input. The noise envelopes generated by employing differential rotor speeds are assessed through the $OSPL_A$. A comparison of the CR and CTR noise envelopes indicates that the CTR configuration exhibits a wider range of noise variation at the same load factor, whereas the CR configuration typically produces a higher maximum noise level across the same range of load factors. It is also found that the drone's noise level is closely related to aerodynamic characteristics of propellers and, potentially, the propeller–propeller interactions that are associated with BVI and slipstream ingestion. Operating the fore propeller at a higher speed than the aft propeller often results in an increased $OSPL_A$ compared to the equal-throttle condition, regardless of whether the propellers are arranged in the CR or CTR configuration. Conversely, a noise reduction is observed when operating the aft propeller at a higher speed than the fore propeller. This reduction is noticeable (at most ~ 4 dBA) only within a limited range of load factors, specifically between 0.6 and 1.1 for the CR configuration and between 0.5 and 0.9 for the CTR configuration. For the CR and CTR configurations, the spectra of SPL_A reveal that the tonal components of the UAV noise often exhibit a haystacking pattern when the fore propellers rotate faster than the aft propellers. Broadband noise appears to be a major contributor to the radiated noise across all loading conditions because of its notable level of SPL_A. It is also worth mentioning that the shaft noise becomes more significant with increasing load factors.

In summary, this study demonstrates the potential for optimizing acoustic–thrust performance through the use of differential rotor speed. The results foster discussion on how differential rotor speed modifies the aerodynamic and aeroacoustic mechanisms of a coaxial system, and they provide guidance for improving the performance and acoustic emissions of a multicopter drone across a range of operating conditions. However, it should be noted that the present findings may be specific to the geometry investigated as installation effects were not isolated in this study. Moreover, future flow-field measurements would be valuable for enhancing the understanding of the physical processes underlying the application of differential rotor speed.

AUTHOR DECLARATIONS

Conflict of Interest

The authors have no conflicts to disclose.

DATA AVAILABILITY

The data that support the findings of this study are available from the corresponding author upon reasonable request.

[1]S. G. Gupta, D. M. Ghonge, and P. M. Jawandhiya, "Review of unmanned aircraft system (UAS)," Int. J. Adv. Res. Comput. Eng. Technol. **2**, 1646–1658 (2013).
[2]M. Hassanalian, A. Abdelkefi, M. Wei, and S. Ziaei-Rad, "A novel methodology for wing sizing of bio-inspired flapping wing micro air vehicles: Theory and prototype," Acta Mech. **228**, 1097–1113 (2017).
[3]Federal Aviation Administration, "FAA Aerospace Forecast Fiscal Years 2023-2043: Unmanned aircraft system and advance air mobility," U.S. Department of Transportation, Washington, DC (2023).
[4]R. O'Connor, "Developing a multirotor UAV platform to carry out research into autonomous behaviours, using on-board image processing techniques," BE thesis, Faculty of Engineering, Computing, and Mathematics, University of Western Australia, 2013.
[5]H. Ubaya and M. Iqbal, "First person view on flying robot for real time monitoring," in *Proceeding of the 1st International Conference on Computer Science and Engineering 2014*, Palembang, Indonesia (September 24–25) (Universitas Sriwijaya, Palembang, Indonesia, 2014).

[6]R. S. McKay, M. J. Kingan, S. T. Go, and R. Jung, "Experimental and analytical investigation of contra-rotating multi-rotor UAV propeller noise," Appl. Acoust. **177**, 107850 (2021).
[7]A. Straubinger, R. Rothfeld, M. Shamiyeh, K.-D. Büchter, J. Kaiser, and K. O. Plötner, "An overview of current research and developments in urban air mobility—Setting the scene for UAM introduction," J. Air Transp. Manage. **87**, 101852 (2020).
[8]P. N. Sorensen and D. R. Cuppoletti, "Rotor-rotor interaction noise of counter-rotating vs co-rotating rotors for air mobility applications," in *AIAA SCITECH 2022 Forum*, San Diego, CA (January 3–7) (American Institute of Aeronautics and Astronautics, Reston, VA, 2022), p. 1296.
[9]M. Malakouti Khah, S. M. Esmailifar, and S. Saadat, "Design and development of a novel multirotor configuration with counter-rotating coaxial propellers," Sci. Rep. **14**(1), 11580 (2024).
[10]A. Weisbrich, J. Godston, and E. Bradley, "Technology and benefits of aircraft counter rotation propellers," NASA Technical Memorandum 82983, National Aeronautics and Space Administration, Washington, DC (1982).
[11]G. Mitchell and D. Mikkelson, "Summary and recent results from the NASA advanced high-speed propeller research program," in *18th Joint Propulsion Conference*, Cleveland, OH (June 21–23) (American Institute of Aeronautics and Astronautics, Reston, VA, 1982), p. 1119.
[12]S. D. Prior, "Reviewing and investigating the use of co-axial rotor systems in small UAVs," Int. J. Micro Air Vehicles **2**(1), 1–16 (2010).
[13]C. P. Coleman, "A survey of theoretical and experimental coaxial rotor aerodynamic research," NASA Technical Paper 3675, National Aeronautics and Space Administration, Washington, DC (1997).
[14]A. Garofano-Soldado, D. Ragni, L. T. L. Pereira, R. Zamponi, A. Ollero, and G. Heredia, "Aerodynamic model of counter-rotating coaxial rotors near the ground," Aerosp. Sci. Technol. **168**, 111112 (2026).
[15]S. A. Rizzi, D. L. Huff, D. D. Boyd, P. Bent, B. S. Henderson, K. A. Pascioni, D. C. Sargent, D. L. Josephson, M. Marsan, H. B. He, and R. Snider, "Urban air mobility noise: Current practice, gaps, and recommendations," NASA Technical Publication TP-20205007433, National Aeronautics and Space Administration, Washington, DC (2020).
[16]European Union Aviation Safety Agency, "Study on the societal acceptance of urban air mobility in Europe," European Union Aviation Safety Agency, Cologne, Germany (2021).
[17]L. Babetto, A. Kirste, J. Deng, M. Husemann, and E. Stumpf, "Adoption of the urban air mobility system: Analysis of technical, legal and social aspects from a European perspective," J. Air Transp. Res. Soc. **1**(1), 152–174 (2023).
[18]N. L. Schatzman, "Aerodynamics and aeroacoustic sources of a coaxial rotor," NASA Technical Memorandum NASA/TM-2018-219895, National Aeronautics and Space Administration, Washington, DC (2018).
[19]M. S. McCluer, "Helicopter blade-vortex interaction noise with comparisons to CFD calculations," NASA Technical Memorandum 110423, National Aeronautics and Space Administration, Washington, DC (1996).
[20]H. Y. Yung, "Rotor blade–vortex interaction noise," Prog. Aerosp. Sci. **36**(2), 97–115 (2000).
[21]Y. Hong, D. Lee, S. Yang, H. Kook, and K. Yee, "Exploration of stacked rotor designs for aerodynamics in hover," Aerosp. Sci. Technol. **141**, 108557 (2023).
[22]R. Zamponi, G. Gioli Torrione, V. Zůbek, E. Gallo, A. Zarri, and C. Schram, "Maneuvering drone noise investigation in a reverberant environment," J. Acoust. Soc. Am. **157**(6), 4468–4481 (2025).
[23]N. S. Zawodny, D. D. Boyd, Jr., and C. L. Burley, "Acoustic characterization and prediction of representative, small-scale rotary-wing unmanned aircraft system components," in *American Helicopter Society (AHS) Annual Forum*, NF1676L-22587, West Palm Beach, FL (May 17–19) (Vertical Flight Society, Fairfax, VA, 2016).
[24]L. Chen, T. Batty, M. Giacobello, and R. Widjaja, "Prediction of small-scale rotor noise using a low-fidelity model-based framework," in *Proceedings of ACOUSTICS*, Cape Schanck, Australia (November 10–13) (Australian Acoustical Society, Melbourne, VIC, 2019), Vol. 10.
[25]S. Lee, L. Ayton, F. Bertagnolio, S. Moreau, T. P. Chong, and P. Joseph, "Turbulent boundary layer trailing-edge noise: Theory, computation, experiment, and application," Prog. Aerosp. Sci. **126**, 100737 (2021).
[26]T. Sinnige, T. C. Stokkermans, D. Ragni, G. Eitelberg, and L. L. Veldhuis, "Aerodynamic and aeroacoustic performance of a propeller propulsion system with swirl-recovery vanes," J. Propul. Power **34**(6), 1376–1390 (2018).
[27]N. Peake and A. B. Parry, "Modern challenges facing turbomachinery aeroacoustics," Annu. Rev. Fluid Mech. **44**(1), 227–248 (2012).
[28]D. B. Hanson, "Noise of counter-rotation propellers," J. Aircraft **22**(7), 609–617 (1985).
[29]M. Kingan and A. Parry, "Acoustic theory of the many-bladed contra-rotating propeller: Analysis of the effects of blade sweep on wake interaction noise," J. Fluid Mech. **868**, 385–427 (2019).
[30]M. J. Kingan, "Open rotor broadband interaction noise," J. Sound Vib. **332**(17), 3956–3970 (2013).
[31]A. J. Landgrebe and E. D. Bellinger, "Experimental investigation of model variable-geometry and ogee tip rotors," NASA Contractor Report 2275, National Aeronautics and Space Administration, Washington, DC (1974).
[32]J. B. Rorke, "Hover performance tests of full scale variable geometry rotors," NASA Contractor Report NASA-CR-2713, National Aeronautics and Space Administration, Washington, DC (1976).
[33]W. Dobrzynski, "Propeller noise reduction by means of unsymmetrical blade-spacing," J. Sound Vib. **163**(1), 123–126 (1993).
[34]W. Dobrzynski, "Unsymmetrical blade-spacing propeller noise reduction without performance penalty," in *INTER-NOISE and NOISE-CON Congress and Conference Proceedings*, Newport Beach, CA (December 4–6) (Institute of Noise Control Engineering USA, Reston, VA, 1989), Vol. 1989, pp. 255–258.
[35]W. Dobrzynski, "Aeroacoustic wind-tunnel tests on full-scale propellers with unsymmetrical blade spacing," in *Inter-Noise 90; Proceedings of the International Conference on Noise Control Engineering*, Göteborg, Sweden (August 27–30) (International Institute of Noise Control Engineering, West Lafayette, IN, 1990), Vol. 1, pp. 475–478.
[36]E. Grande, S. Shubham, F. Avallone, D. Ragni, and D. Casalino, "Computational aeroacoustic study of co-rotating rotors in hover," Aerosp. Sci. Technol. **153**, 109381 (2024).
[37]D. Uehara, J. Sirohi, and M. J. Bhagwat, "Hover performance of corotating and counterrotating coaxial rotors," J. Am. Helicopter Soc. **65**(1), 1–8 (2020).
[38]C. E. Tinney and J. Valdez, "Thrust and acoustic performance of small-scale, coaxial, corotating rotors in hover," AIAA J. **58**(4), 1657–1667 (2020).
[39]S. Whiteside, N. Zawodny, X. Fei, N. A. Pettingill, M. D. Patterson, and P. Rothhaar, "An exploration of the performance and acoustic characteristics of UAV-scale stacked rotor configurations," in *AIAA Scitech 2019 Forum*, San Diego, CA (January 7–11) (American Institute of Aeronautics and Astronautics, Reston, VA, 2019), p. 1071.
[40]L. T. L. Pereira, B. Puroja, R. Zamponi, I. Rosa, and D. Ragni, "Aeroacoustic measurements of a contra-rotating UAV vehicle," in *INTER-NOISE and NOISE-CON Congress and Conference Proceedings*, Chiba, Japan (August 20–23) (Institute of Noise Control Engineering, West Lafayette, IN, 2023), Vol. 268, pp. 5175–5184.
[41]H. Fletcher and W. A. Munson, "Loudness, its definition, measurement and calculation," Bell Syst. Tech. J. **12**(4), 377–430 (1933).
[42]X. Zhao, N.-Z. Huang, X. Liang, P. Zhou, W.-P. Song, and Y.-F. Lin, "The aerodynamic performance measurement of coaxial rotor in hover," in *31st Congress of the International Council of the Aeronautical Sciences, ICAS 2018*, Belo Horizonte, Brazil (September 9–14) (International Council of the Aeronautical Sciences, Belo Horizonte, Brazil, 2018), paper no. ICAS2018_0470.
[43]O. Dantsker, M. Caccamo, R. W. Deters, and M. S. Selig, "Performance testing of aero-naut cam folding propellers," in *AIAA Aviation 2020 Forum*, Virtual Conference (June 15–19) (American Institute of Aeronautics and Astronautics, Reston, VA, 2020), p. 2762.
[44]O. D. Dantsker, M. Caccamo, R. W. Deters, and M. Selig, "Performance testing of APC electric fixed-blade UAV propellers," in *AIAA Aviation 2022 Forum*, Chicago, IL (June 27–July 1) (American Institute of Aeronautics and Astronautics, Reston, VA, 2022), p. 4020.
[45]P. Welch, "The use of fast Fourier transform for the estimation of power spectra: A method based on time averaging over short, modified periodograms," IEEE Trans. Audio Electroacoust. **15**(2), 70–73 (1967).
[46]T. Zhou, H. Jiang, and B. Huang, "Quad-copter noise measurements under realistic flight conditions," Aerosp. Sci. Technol. **124**, 107542 (2022).
[47]F. De Gregorio, K. Rossignol, G. Ceglia, and J. Yin, "Aerodynamic and acoustic interactional effects for small commercial propellers in co-axial

counter-rotating arrangements," Aerosp. Sci. Technol. **159**, 110001 (2025).
[48]A. F. Deming, "Propeller rotation noise due to torque and thrust," J. Acoust. Soc. Am. **12**(1), 173–182 (1940).
[49]D. W. Kurtz and J. E. Marte, "A review of aerodynamic noise from propellers, rotors, and lift fans," NASA Contractor Report NASA-CR-107568, National Aeronautics and Space Administration, Washington, DC (1970).
[50]L. M. Shaw and J. R. Balombin, "Rotor wake characteristics relevant to rotor-stator interaction noise generation," J. Aircraft **19**(11), 954–962 (1982).
[51]S. Glegg and W. Devenport, *Aeroacoustics of Low Mach Number Flows: Fundamentals, Analysis, and Measurement* (Academic Press/Elsevier, London, UK, 2017).
[52]A. Cooke and E. Fitzpatrick, *Helicopter Test and Evaluation* (John Wiley & Sons, Hoboken, NJ, 2009).
[53]H. H. Murray IV, W. J. Devenport, W. N. Alexander, S. A. Glegg, and D. Wisda, "Aeroacoustics of a rotor ingesting a planar boundary layer at high thrust," J. Fluid Mech. **850**, 212–245 (2018).
[54]A. McAlpine and B. J. Tester, "Spectral broadening of tonal sound propagating through an axisymmetric turbulent shear layer," AIAA J. **58**(3), 1093–1106 (2020).
[55]F. Petricelli, P. Chaitanya, S. Palleja-Cabre, S. Meloni, P. F. Joseph, A. Karimian, S. Palani, and R. Camussi, "An experimental investigation on the effect of in-flow distortions of propeller noise," Appl. Acoust. **214**, 109682 (2023).
[56]N. S. Jamaluddin, A. Celik, K. Baskaran, D. Rezgui, and M. Azarpeyvand, "Experimental analysis of a propeller noise in turbulent flow," Phys. Fluids **35**(7), 075106 (2023).
[57]D. Qin, O. Stalnov, and X. Huang, "Numerical investigation of parameters influencing the turbulence-ingesting noise of a ten-bladed propeller," Ocean Eng. **300**, 117237 (2024).
[58]A. Piccolo, R. Zamponi, F. Avallone, and D. Ragni, "Modification of Amiet's model for turbulence-ingestion noise prediction in rotors," J. Acoust. Soc. Am. **158**(1), 461–475 (2025).
[59]D. Uehara and J. Sirohi, "Quantification of swirl recovery in a coaxial rotor system," in *Proceedings of the American Helicopter Society 73rd Annual Forum*, Fort Worth, TX (May 9–11) (Vertical Flight Society, Fairfax, VA, 2017), pp. 9–11.
[60]J. Yana and O. Rand, "Performance analysis of a coaxial rotor system in hover: Three points of view," in *28th International Congress of the Aeronautical Sciences*, Brisbane, Australia (September 23–28) (International Council of the Aeronautical Sciences, Bonn, Germany, 2012).
[61]J. Ko and S. Lee, "Numerical investigation of inter-rotor spacing effects on wake dynamics of coaxial rotors," J. Aircraft **58**(2), 363–373 (2021).